Research Article E-ISSN: 2707-6261 RAFT Publications

Lybian Journal of Basic Sciences

Numerical Experimental for an Inverse Source Problem Method

Abdalkaleg Atia Idris Hamad

Department of Mechanical Engineering, Faculty of Engineering, Omar Al-Mukhtar University, El-Bieda, Libya

***Correspondence:** Abdalkaleg Atia Idris Hamad, Department of Mechanical Engineering, Faculty of Engineering, Omar Al-Mukhtar University, El-Bieda, Libya, Email: abdalkaleg.hamad@omu.edu.ly

Received: 17 Jun 2021 **Accepted: 22 Jul 2021** **Published: 25 Aug 2021**

DOI: https://doi.org/10.36811/ljbs.2021.110074

Citation: Abdalkaleg Atia Idris Hamad. 2021. Numerical Experimental for an Inverse Source Problem Method. LJBS. 5: 125-139.

Abstract

This paper examines extensions of an iterative method for inverse evaluation of the source function for two elliptic systems. The method begins with a starting value for the undetermined source. Next, a background field and equations for the error field are obtained. 2-D domains are considered. This method is suitable for Helmholtz and Poisson operators. In the presence of finite-difference grid resolution, a varying amount of boundary data, and methods of filtering the noise in the boundary data and the noise intensity of the boundary data, the performance, accuracy, and iteration count of the algorithm are investigated.

Keywords: Source, Inverse Problems, Poisson, Noise, Ill-Posedness, Well-Posed

Introduction

The method is a numerical method to determine the source function for an elliptic system in two and three dimensions (*1*). This problem occurs in the general area of non-invasive imaging techniques that have noticed an expanded amount of utility and applications in various fields of sciences. For example, in diffuse optical tomography (*2*). One seeks to investigate neuronal activity in the living human brain. In bioluminescence imaging, biological entities (e.g. tumor cells) are tagged with luciferase enzymes and implanted in a small animal (*3*).

In this paper, the convergence of the method with the grid sizes is examined. Also, some parts of the boundary are not accessible, and it is impossible to measure either flux (or Neumann boundary) and Dirichlet conditions at these parts of the boundaries are assumed. The inverse source problem method in (*1*) with respect to missing some data at the boundaries (limited number of the sensors at the boundaries) and compare to the case where the number of the sensors can be assumed unlimited is studied. The missing data at the boundaries are recovered by fit a polynomial of degree n to the available data. In Section 2, the

algorithm for recovering the source of the Poisson equation in the two-dimensional domain is briefly introduced. In section 3, the method for a 2-D domain is developed. In section 4, the grid size to study the convergence of the method is varied. Then the inverse source method with no noisy data, an unlimited number of sensors, and the method limited number of sensors at the boundaries is examined (*4*). Lastly, the method with different filtering noisy data methods was examined.

Convergence with grid size and iteration

Convergence with grid size and iteration

Consider an inverse source problem in a two-dimensional domain. Assume that the actual source term in Eq. [1] is given by

$$u_{xx} + u_{yy} = 1 + g(x)f(y) \quad \text{in } \Omega, \qquad [1]$$

where a unit square and the variable u(x) can be the electric potential or the material temperature. The boundary is accessible, and it is possible to measure both flux (or Neumann boundary) and Dirichlet conditions on the boundary $\partial\Omega$. Starting with an assumed value for the source term $1 + \hat{g}(x)\hat{f}(y)$.

$$g(x)f(y) = \left[1 + \exp\left(\frac{(x-0.3)^4}{0.00001}\right)\right]\left[1 + 2\exp\left(\frac{(y-0.65)^4}{0.00001}\right)\right]. \qquad [2]$$

In this section, the convergence of the method with grid size is studied. As is expected the convergence of the method is improving as the grid size is decreased. Because the error of the approximation by finite differences is proportional to the grid size. Figure 1 shows the reduction of the source error given by [2-3] with different grid sizes. The convergence rate of the source error is increasing as the grid sizes decreasing.

$$Error1 = \int_{\Omega} \left[g(x)f(y) - \hat{g}(x)\hat{f}(y)\right]^2, \qquad [3]$$

$$Error2 = \int_{\Omega} [\nabla_n(u(\mathbf{x})) - \nabla_n(\hat{u}(\mathbf{x}))]^2, \qquad [4]$$

Where error 1 is to study the error in the recovered unknown function. Error 2 is to study the difference between the given data, and the calculated value at a given iteration. Figure 2 shows the reduction of the error 2. The figure, 2 shows the reduction of error between the given data at the boundaries and the computed values by this method.

The convergence of the recovered functions in the x-direction and the y-direction with different grid sizes are shown in Figures 3 and 4, respectively. Decreasing the grid sizes gives a close approximation for the unknown sources.

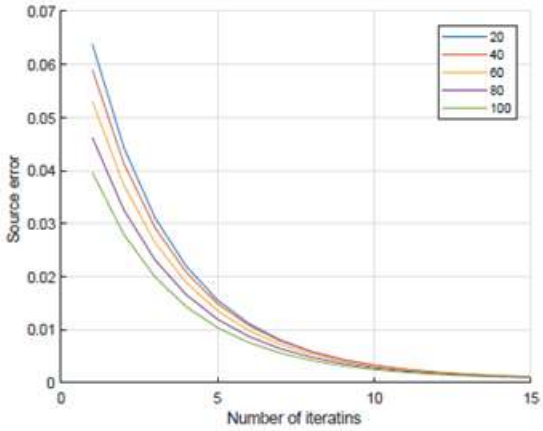

Figure 1: The reduction of the source error given by Eq. [3].

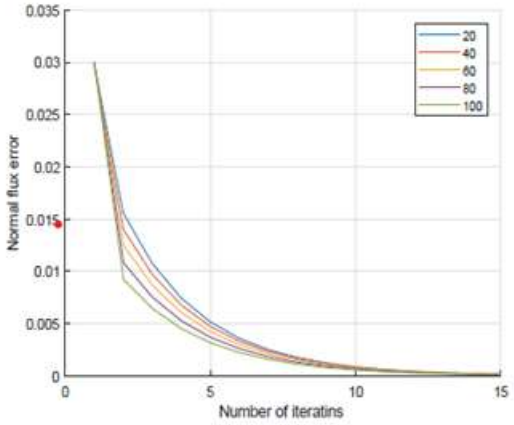

Figure 2: The reduction of the source error given by Eq. [4].

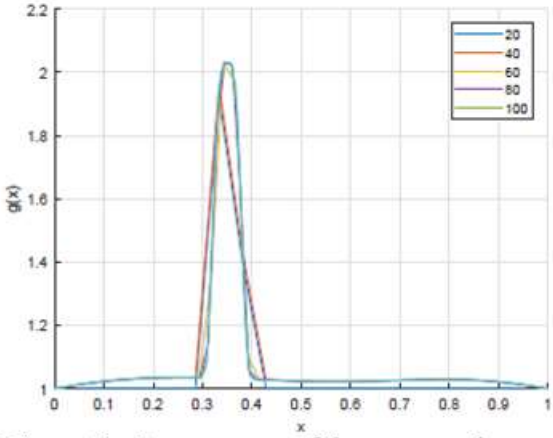

Figure 3: Convergence of the recovered source function in the x-direction

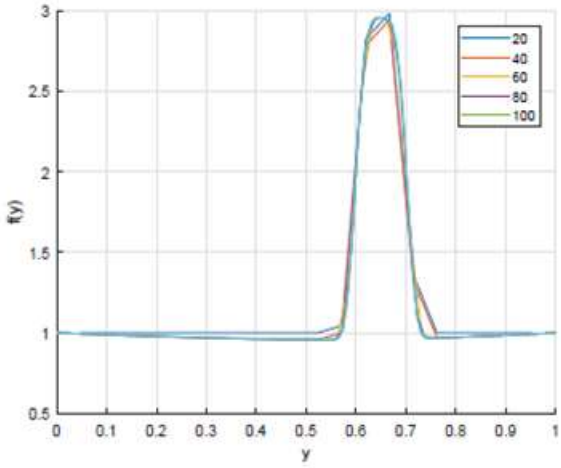

Figure 4: Convergence of the recovered source function in the y-direction

The inverse source method with no noise data and a limited number of sensors

Consider an inverse source problem in a two-dimensional domain. Assume that the actual source term in Eq. [1] is given by Eq. [2].

The method with a limited number of sensors in two cases. First, when the collected data on one side is 78% of the full data. Two experiments have been done one at x=1, and another at y=1. Second, when the collected data on all sides are 78% of the full data is studied.

First missing data on one side.

The limitations of measuring the u_x at the boundaries lead to missing data. The missing data is estimated by using a 10-degree polynomial.

Missing data on one side at $x = 1$

Figure 5 shows the full collected data and 78% of the full data after the estimation of the missing data is made.

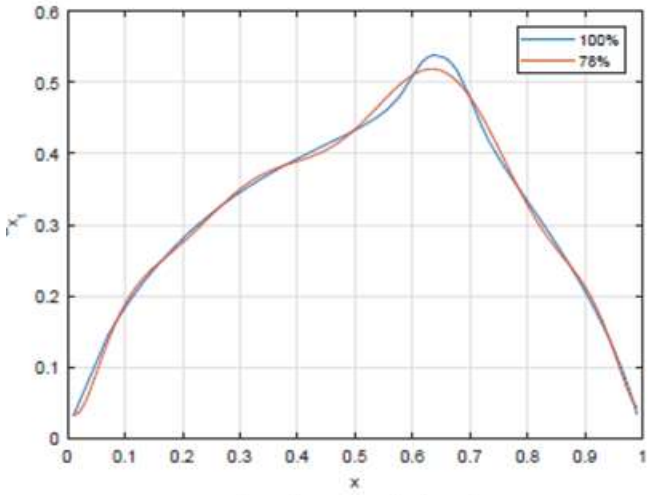

Figure: (5). Estimation of missing data at x=1.

Figure 6 shows the reduction in error 1 for the full collected data and 78% of the full data.

Figure 7 shows the reduction in error 2 for the full collected data and 78% of the full data.

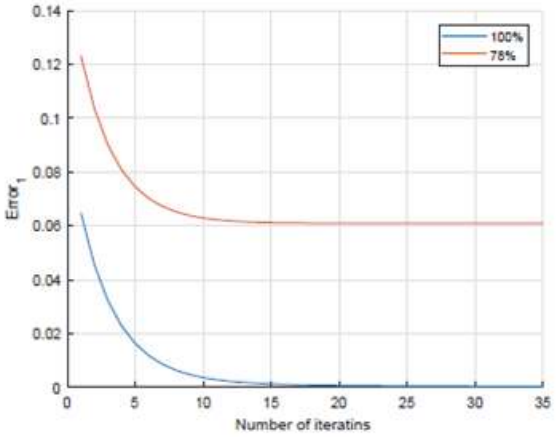

Figure 6: The reduction of error 2 with missing data at x=1.

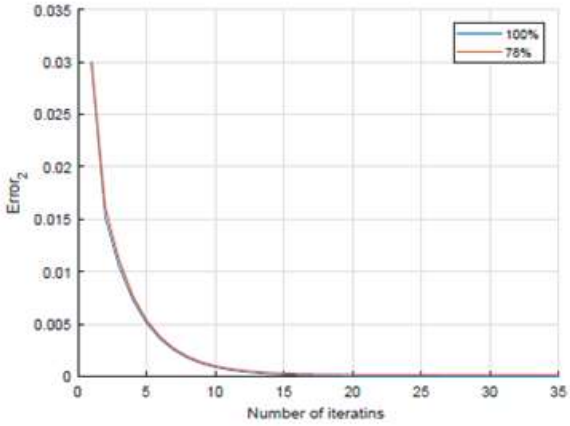

Figure 7: The reduction of error 2 with missing data at x=1.

Figures 8 and 9 show the recovered functions after a few iterations with 78% of the full data and full data at x=1 and compare them to the actual source functions.

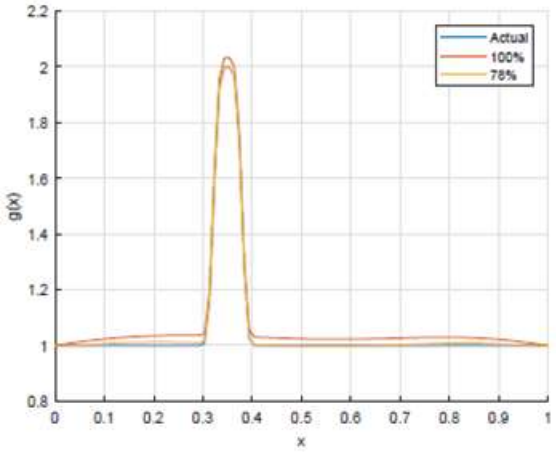

Figure 8: Convergence of the recovered source function in the x-direction with missing data at x=1.

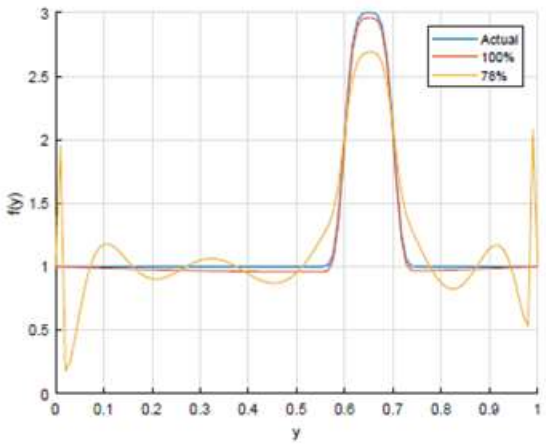

Figure 9: Convergence of the recovered source function in the y-direction with missing data at x=1.

Figure 10 shows the recovered source function after 35 iterations with 78% of full data at x=1. Next, the method when there are limited numbers of sensors at y=1 is studied.

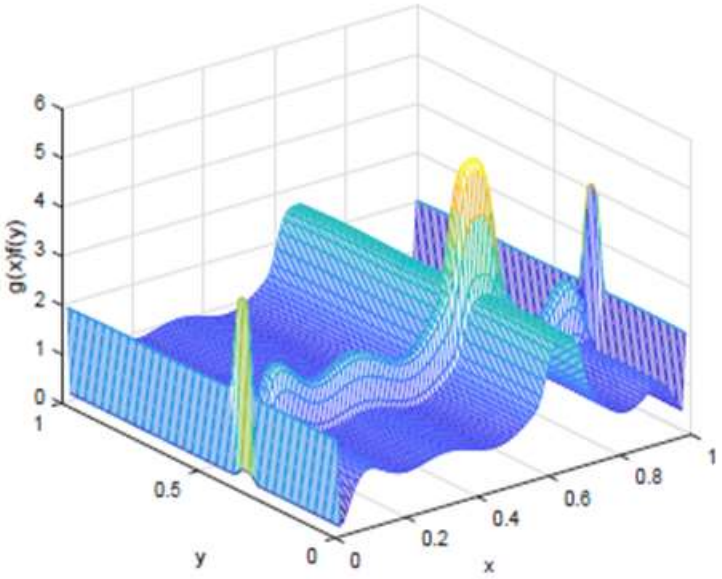

Figure 10: Recovered source function with missing data at x=1.

Missing data on one side at y=1

Figure 11 shows the full collected data and 78% of the full data after the estimation of the missing data is made.

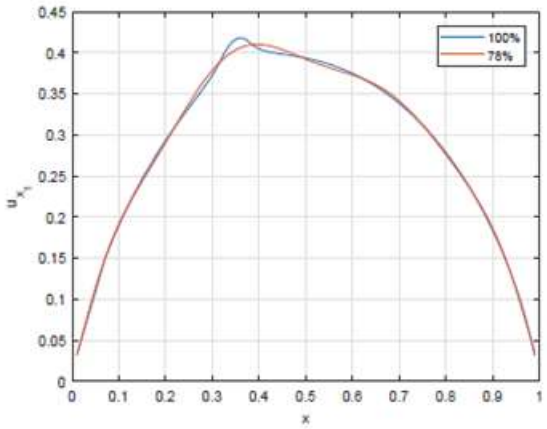

Figure 11: Estimation of missing data at y=1.

Figure 12 shows the reduction in error 1 for the full collected data and 78% of the full data.
Figure 13 shows the reduction in error 2 for the full collected data and 78% of the full data.

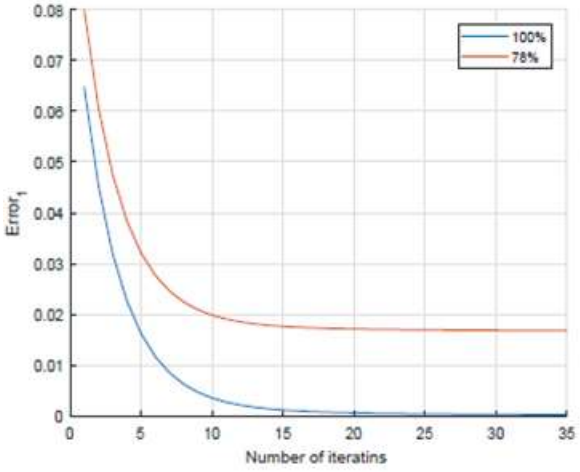

Figure: (12). The reduction of error 2 with missing data at y=1.

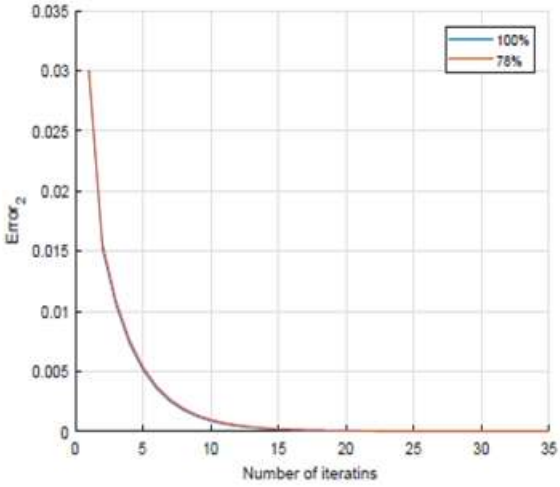

Figure: (13). The reduction of error 2 with missing data at y=1.

Figures 14 and 15 show the recovered functions after a few iterations with 78% of the full data and full data at y=1 and compare them to the actual source functions.

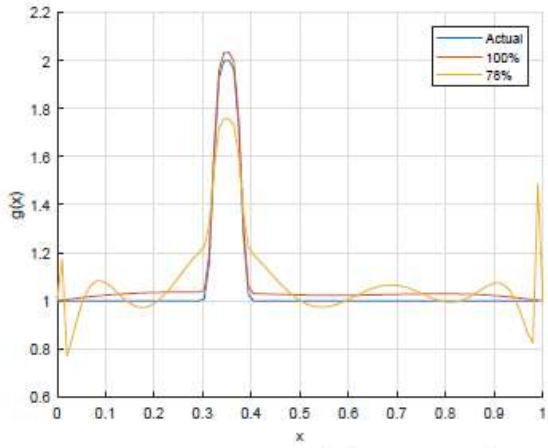

Figure 14: Convergence of the recovered source function in the x-direction

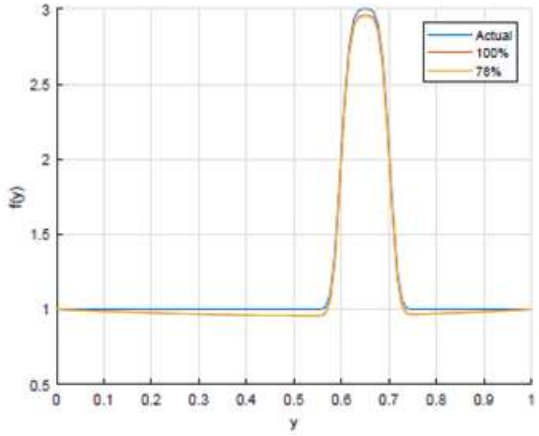

Figure 15: Convergence of the recovered source function in the y-direction

Figure 16 shows the recovered source function after 35 iterations with 78% of full data at y=1.

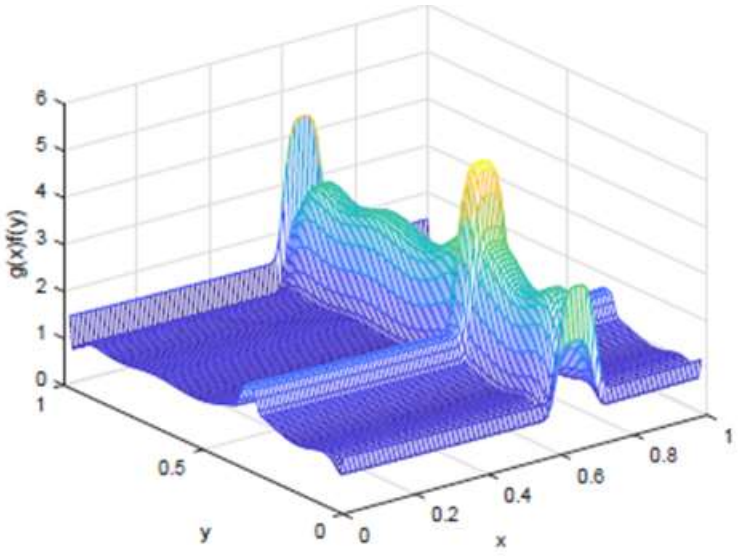

Figure 16: Recovered source function with missing data at y=1.

Second missing data on all sides

Figures 17-20 show the full collected data and 78% of the full data for all sides after the estimation of the missing data is made.

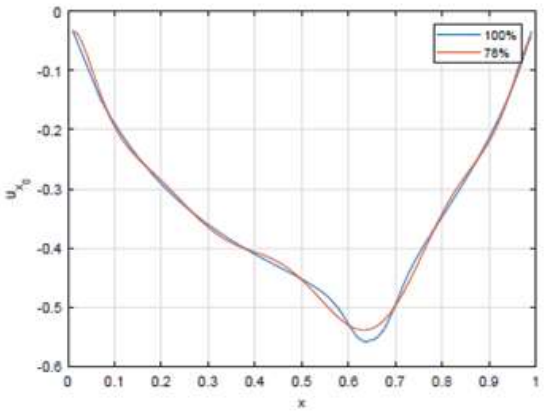

Figure 17: Estimation of missing data at x=0.

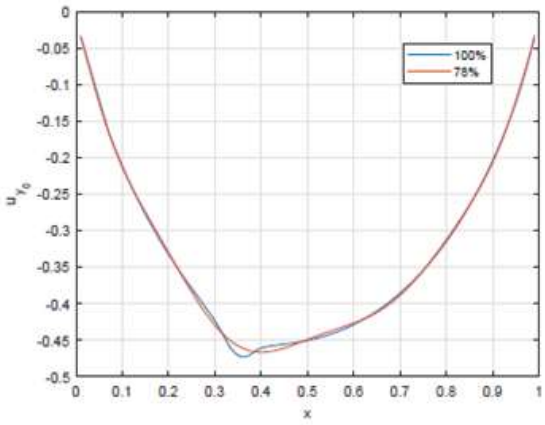

Figure 18: Estimation of missing data at y=0.

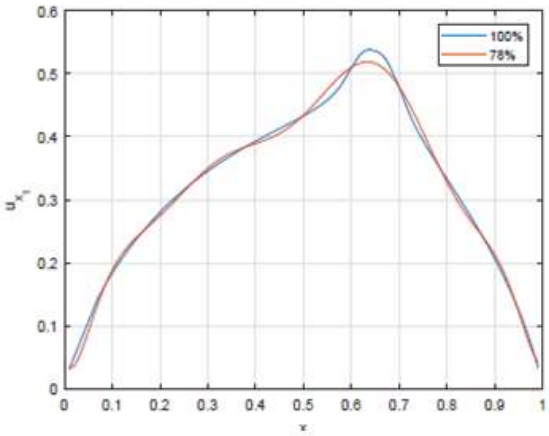

Figure 19: Estimation of missing data at x=1.

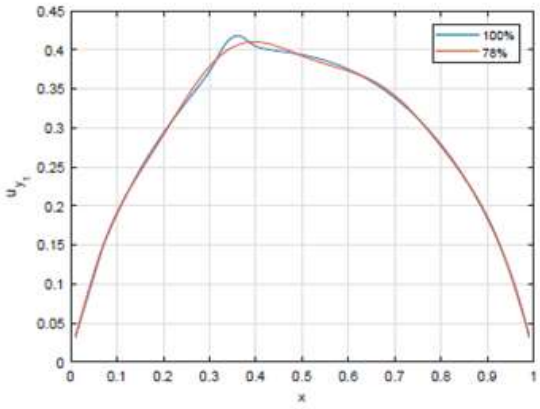

Figure 20: Estimation of missing data at y=1.

Figures 21, 22 and 23 show the estimation of 75%, 50%, and 25% missing data, respectively at x=0.

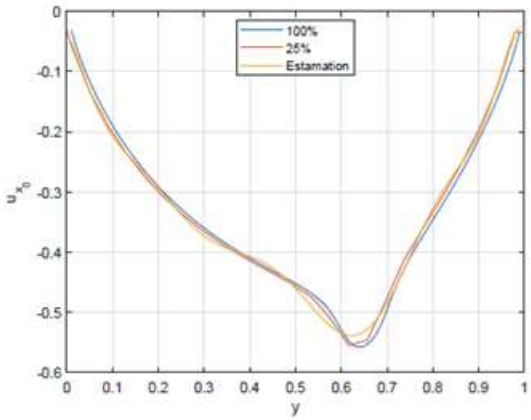

Figure 21: Estimation of 75% missing data at x=0.

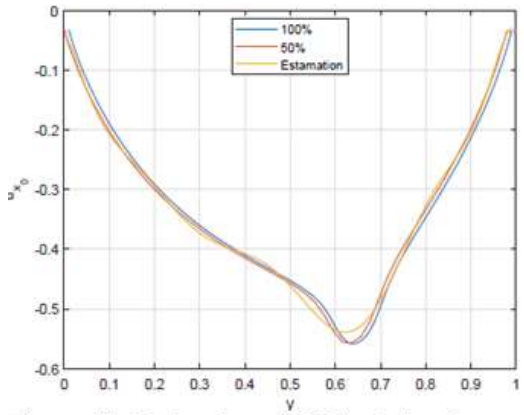

Figure 22: Estimation of 50% missing data at x=0.

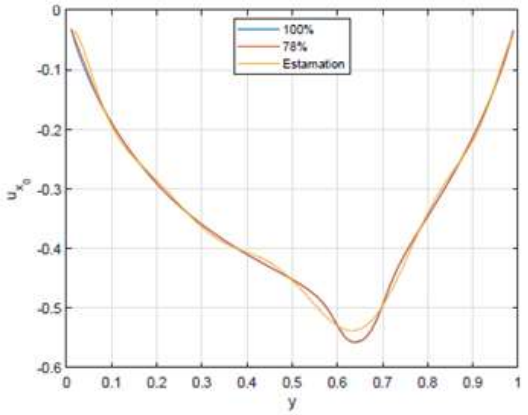

Figure 23: Estimation of 22% missing data at x=0.

Figures 24, 25, and 34 show the estimation of 75%, 50%, and 22% missing data, respectively at y=0.

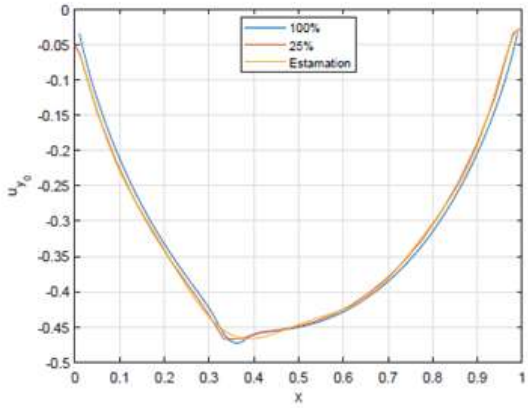

Figure 24: Estimation of 75% missing data at y=0.

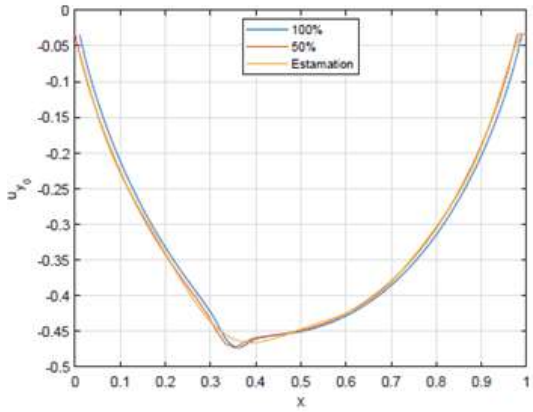

Figure 25: Estimation of 50% missing data at y=0.

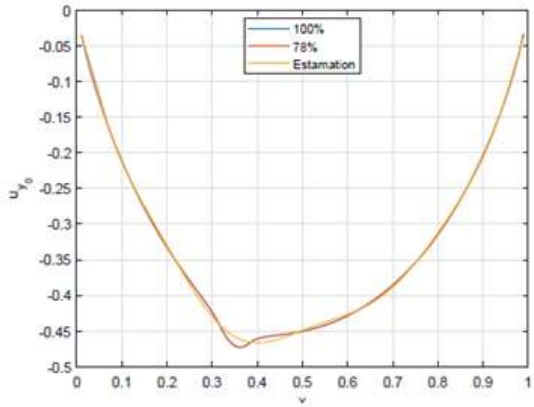

Figure 26: Estimation of 22% missing data at y=0.

Figures 27, 28, and 29 show the estimation of 75%, 50%, and 25% missing data, respectively at x=1.

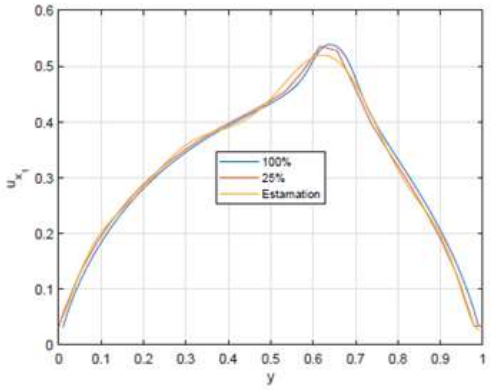

Figure 27: Estimation of 75% missing data at x=1.

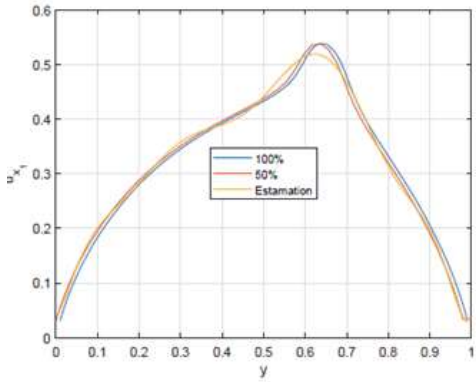

Figure 28: Estimation of 50% missing data at x=1.

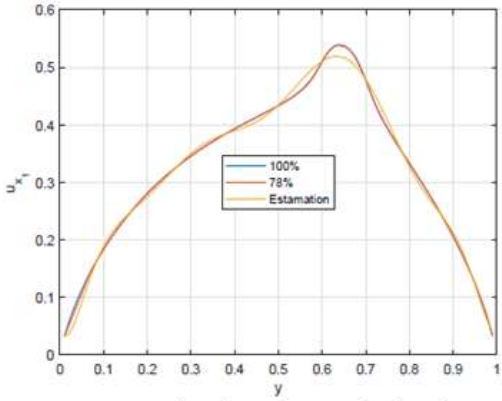

Figure 29: Estimation of 22% missing data at x=1.

Figures 30, 3, and 32 show the estimation of 75%, 50%, and 25% missing data, respectively at y=1.

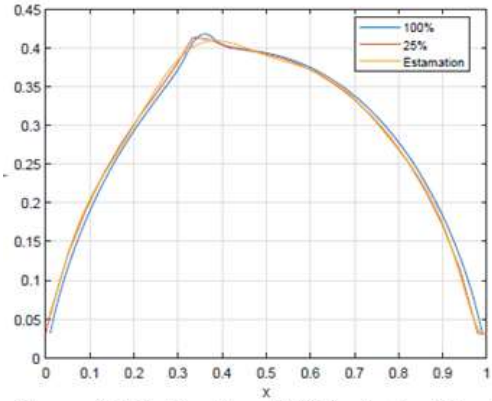

Figure 30: Estimation of 75% missing data at y=1.

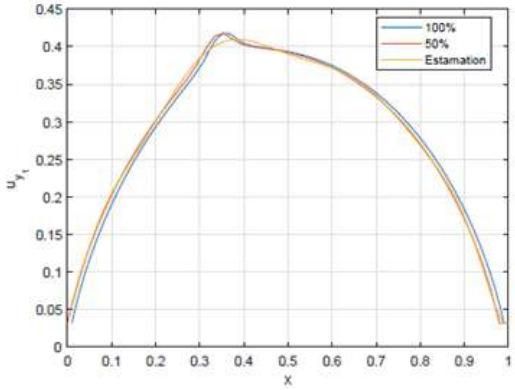

Figure 31: Estimation of 50% missing data at y=0

Figures 32-36 show the full collected data and the 78%, 50%, and 25% of the full data for all sides after the estimation of the missing data is made.

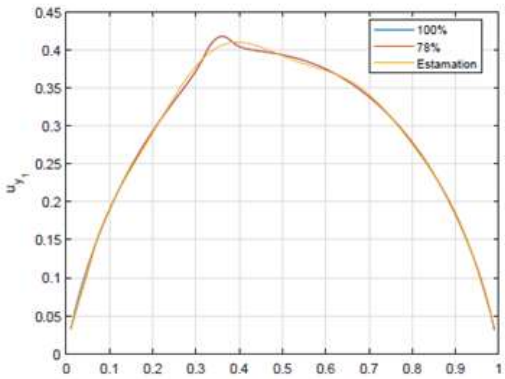

Figure 32: Estimation of 22% missing data at y=0.

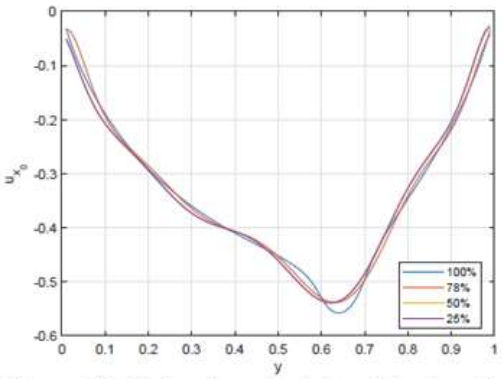

Figure 33: Estimation of missing data at x=0.

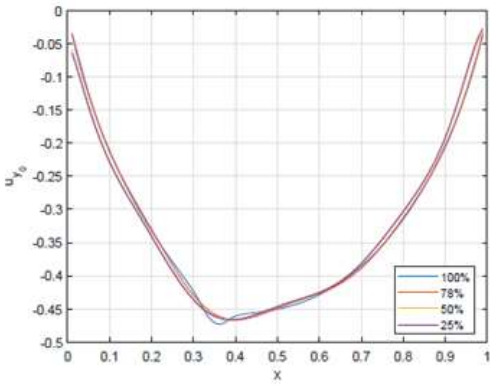

Figure 34: Estimation of missing data at y=0.

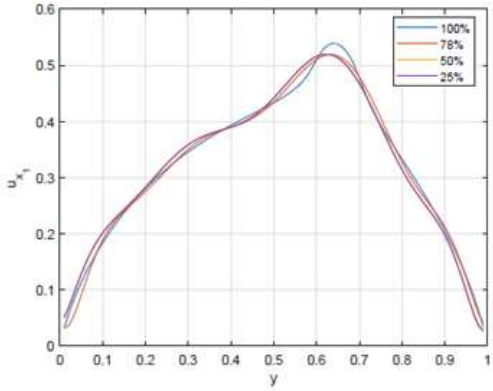

Figure 35: Estimation of missing data at x=1.

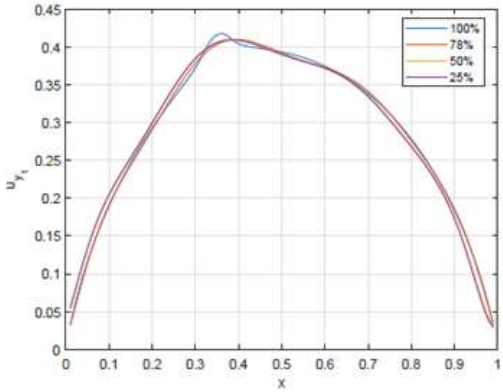

Figure 36: Estimation of missing data at y=1.

Figure 37 shows the reduction in the source error for the full collected data and 78%, 50%, and 25% of the full data for all sides. Here the source error has almost the same convergence rate, but the initial error values are increasing as the missing data percentage is increasing.

Figure 38 shows the reduction in normal flux error for full collected data and 78% of the full data for all sides. Here is for missing 50% and 75% of data there is initially overshooting in the normal flux error and then the convergence rates of this error become the same as 78% of the full data and full data.

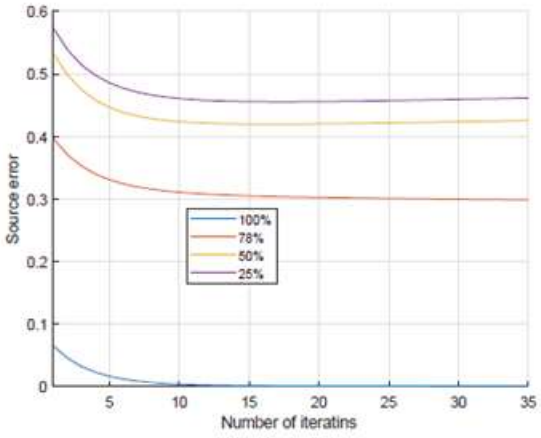

Figure 37: The reduction of the source error with missing data for all sides.

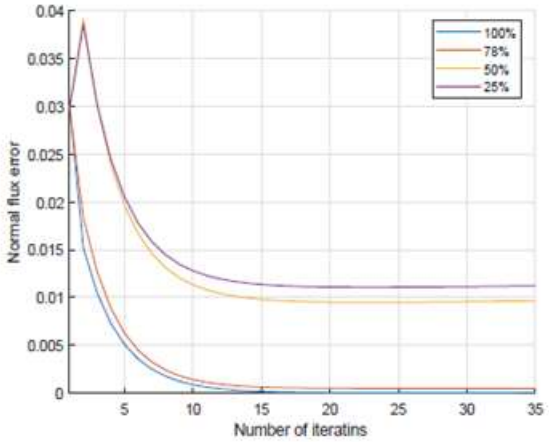

Figure 38: The reduction of normal flux error with missing data for all sides.

Figures 39 and 40 show the recovered functions after 35 iterations with 78% of the full data and full data at all sides and compare them to the actual source functions. Here, the method when the missing data at all the boundaries then according to equations 5 and 17 the estimation of the missing data will affect the correction term $\delta(y)$ and $\sigma(x)$ therefore the recovered function in y- direction and x-direction is studied.

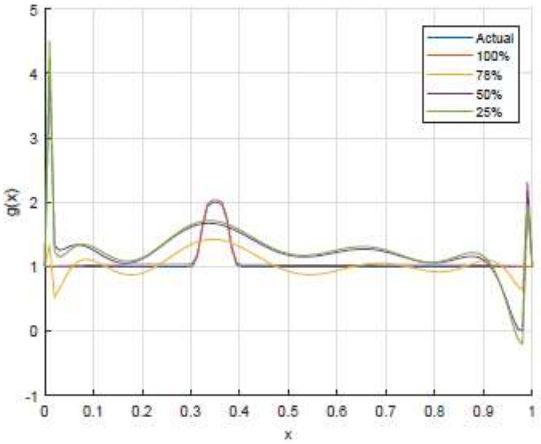

Figure 39: Convergence of the recovered source function in the x-direction

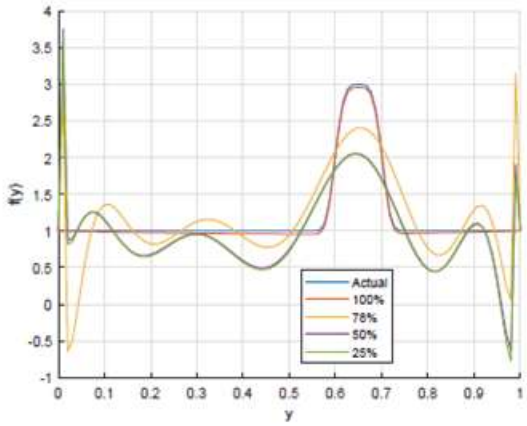

Figure 40: Convergence of the recovered source function in the y-direction.

The inverse source method with different filtering noisy data methods

Briefly, the algorithm with two different methods for filtering the noisy data has been examined. Assuming that the data is noisy, and the signal ratio noise is 5%, the two methods are smooth noisy data and fitting a curved polynomial to noisy data method (*5*, *6*).

Smooth noisy data

In this subsection, before using the data Savitzky-Golay filter is performed to smooth out the data. Basically, Savitzky-Golay filtering can be thought of as a generalized moving average (*7*). To filter data by this method a built-in function in MatLab called smooth data is used (*8*).

Figures 41-44 show the filtering data after performing the Savitzky-Golay filter.

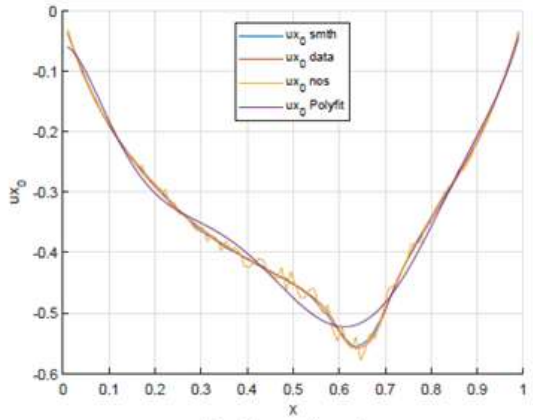

Figure 41: Filtering noisy data at x=0.

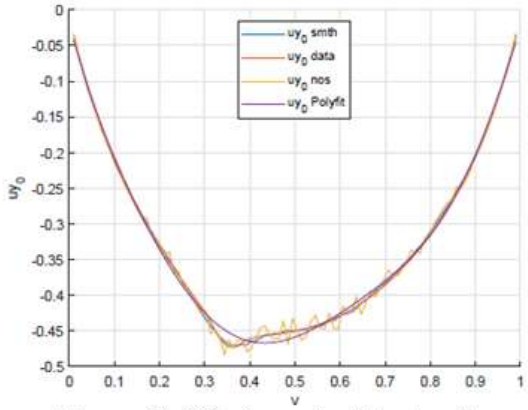

Figure 42: Filtering noisy data at y=0.

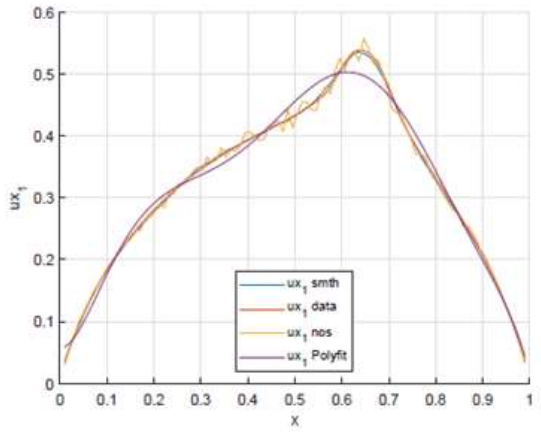

Figure 43: Filtering noisy data at x=1.

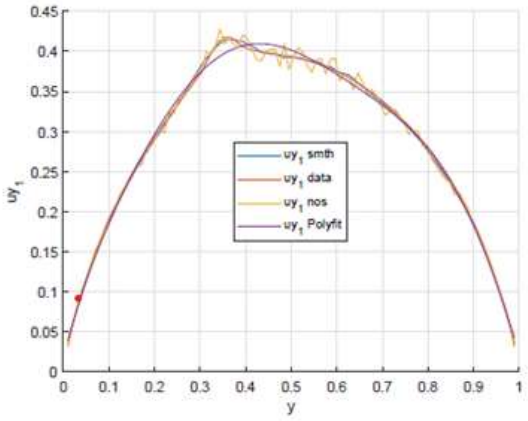

Figure 44: Filtering noisy data at y=1.

Fitting curved polynomial to noisy data method.

The objective of curve fitting is to find the parameters of a mathematical model that describes a set of (usually noisy) data in a way that minimizes the difference between the model and the data. The most common approach is the "linear least squares" method, also called" polynomial least squares" (*9*).

Using a built-in function in MatLab called poly fit to filter data by this method. Figures 41-44 show the filtering data after performing a fitting curved polynomial filter.

Figures 45 and 46 show that the functions of the recovering source with the smooth noisy data filter are better than when the fitting curved polynomial filter is used. Because the Savitzky-Golay smoothing filter is a filter that essentially performs a local polynomial regression but a fitting curved polynomial filter performs a global polynomial regression. These reasons can clearly be seen in Figures 41- 44

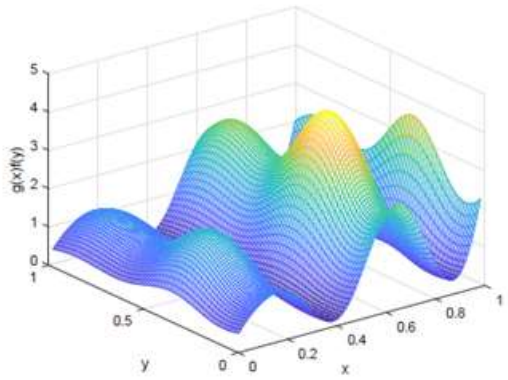

Figure 45: Filtering noisy data by polynomial fitting.

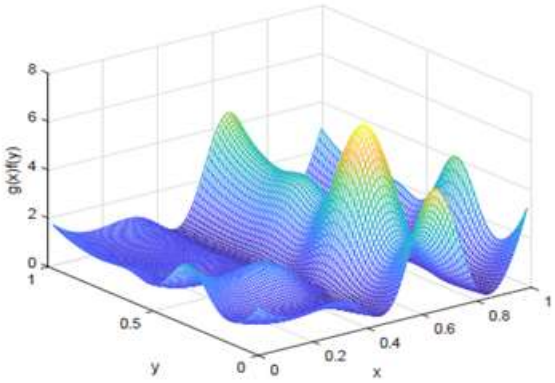

Figure 46: Filtering noisy data with smooth data.

Conclusion

The inverse source problem method for the two-dimensional Poisson equation has been considered. First, the convergence of the method with grid size has been inspected. The convergence of the method is improving as the grid size is decreased.

Second, examining the method when some parts of the boundary are not accessible. Using a simple method to recover the missing data, the unknown functions can be recovered even there is a limited number of sensors on the boundaries. In the case of missing data on one side, the method is working better than the missing data on all sides. If the missing data is at all sides of the domain, the method can recover the location of the source. Because missing data at all sides will affect the correction terms in x and y directions therefor the recovered source functions in x and y directions. This issue might be solved by using a more accurate method to estimate the missing data and changing the positive scalar β.

To examine the method, two different definitions for the reduction of the error are used. The reduction of the source error and normal flux error curves will converge almost at the same number of iterations for both cases (missing data at one side or all sides). Therefore, it can be concluded that the convergence rate of the errors is almost the same for full data and missing data at the boundaries cases.

Third, the results of the methods for two different methods of filtering the noisy data are inspected. The results show that using smooth the noisy data the recovered functions will be better than using fit a polynomial to the noise data.

References

1. A. Hamad, M. Tadi, A numerical method for inverse source problems for Poisson and Helmholtz equations. Physics Letters A 380, 3707 (2016).
2. K. Ren, Recent developments in numerical techniques for transport-based medical imaging methods. Commun. Comput. Phys 8, 1 (2010).
3. S. Li, W. Driessen, S. Sullivan, H. Jiang, Bioluminescence tomography based on phantoms with different concentrations of bioluminescent cancer cells. Journal of Optics A: Pure and Applied Optics 8, 743 (2006).
4. V. Isakov, Inverse problems for partial differential equations. (Springer, 2006), vol. 127.
5. R. Celorrio, A. Mendioroz, A. Salazar, Characterization of vertical buried defects using lock-in vibrothermography: II. Inverse problem. Measurement Science and Technology 24, 065602 (2013).
6. N. C. Roberty, C. J. Alves, On the identification of star-shape sources from boundary measurements using a reciprocity functional. Inverse Problems in Science and Engineering 17, 187 (2009).
7. W. H. Press, S. A. Teukolsky, Savitzky-Golay smoothing filters. Computers in Physics 4, 669 (1990).
8. M. Natick, The MathWorks Inc. MATLAB-Documentation.[online], (2010).
9. T. O'Haver, A pragmatic introduction to signal processing. University of Maryland at College Park, (1997).